Pis'ma v ZhETF, vol. 101, iss. 12, pp. 902 – 907 June 25

Measurements of anisotropic mass of magnons confined in a harmonic trap in superfluid ^{3}He–B

V. V. Zavjalov[1)], *S. Autti, V. B. Eltsov, P. J. Heikkinen*

Low Temperature Laboratory, Department of Applied Physics, Aalto University, PO Box 15100, FI-00076 AALTO, Finland

Submitted 6 May 2015

We can pump magnons to a nearly harmonic magneto-textural trap in superfluid ^{3}He–B. Using the NMR spectroscopy of levels in the trap we have measured the anisotropic magnon mass and related values of the spin-wave velocities. Based on our measurements we provide values of the Fermi-liquid parameter F_1^a.

DOI: 10.7868/S0370274X15120061

Introduction. ^{3}He–B is the topological superfluid with gapless Majorana fermions on the boundary (see recent review [1]). Optical magnons in a magneto-textural trap proved to be a useful and convenient experimental tool for studying various properties of superfluid ^{3}He–B. A number of effects can be observed in this system such as Bose–Einstein condensation of magnons [2], Suhl instability [3] with excitation of other spin-wave modes including a longitudinal Higgs mode [4], self-localization of magnons [5]. It can be used as a probe of quantized vortices [6], Andreev bound states and gravity waves on the ^{3}He surface [7], boundary between ^{3}He–A and ^{3}He–B superfluids [8]. It also can be used as a tool for accurate measurements of various ^{3}He parameters and as a thermometer which works below 0.3 mK [8].

For proper interpretation of these measurements, basic properties of magnons should be accurately known. In this paper we report detailed measurements of magnon spectra from which we find the anisotropic magnon mass and spin-wave velocity in ^{3}He–B.

Spin waves in ^{3}He–B. The equilibrium state of superfluid ^{3}He-B is described by the order parameter matrix:

$$A_{aj} = \frac{1}{\sqrt{3}}\ \Delta\ e^{i\varphi} R_{aj}, \tag{1}$$

where Δ is the energy gap, φ is the phase, and R_{aj} is a rotation matrix which can be written in terms of the rotation axis $\mathbf{n}$ and the angle θ as

$$R^0_{aj} = \cos\theta\ \delta_{aj} + (1-\cos\theta)\ n_a n_j - \sin\theta\ e_{ajk} n_k. \tag{2}$$

In non-zero magnetic fields the gap becomes anisotropic, but for fields used in this work we can neglect this effect.

Spin waves in ^{3}He–B correspond to oscillations of the rotation matrix R_{aj}. The motion is affected by the energy of the spin-orbit interaction F_{so} and the gradient energy F_∇:

$$F_{so} = \frac{\chi_B \Omega_B^2}{15\gamma^2}(R_{jj}R_{kk} + R_{jk}R_{kj}), \tag{3}$$

$$F_\nabla = \frac{1}{2}\Delta^2(K_1 G_1 + K_2 G_2 + K_3 G_3), \tag{4}$$

where

$$G_1 = \nabla_j R_{ak} \nabla_j R_{ak},$$
$$G_2 = \nabla_j R_{ak} \nabla_k R_{aj},$$
$$G_3 = \nabla_j R_{aj} \nabla_k R_{ak},$$

χ_B is the spin susceptibility of the ^{3}He–B, γ – the gyromagnetic ratio for the ^{3}He atom, Ω_B – the Leggett frequency, and K_1, K_2 and K_3 are parameters of the gradient energy.

The linear equation of small spin oscillations near the equilibrium value $\mathbf{S}^0 = (\chi_B/\gamma)\ \mathbf{H}$ is [9]

$$\ddot{S}_c = [\dot{\mathbf{S}} \times \gamma\mathbf{H}]_c + \\ + \frac{\Delta^2\gamma^2}{\chi_B}\left[K\ \nabla^2\ S_c - K'\ \nabla_j R^0_{cj} R^0_{ak} \nabla_k\ S_a\right] - \\ - \Omega_B^2\ \hat{\mathbf{n}} \cdot (\mathbf{S} - \mathbf{S^0})\ \hat{n}_c, \tag{5}$$

where $K = 2K_1 + K_2 + K_3$ and $K' = K_2 + K_3$.

In a texture where $\mathbf{n}$ is almost parallel to $\mathbf{H}$ or in a high magnetic field $\omega_L = |\gamma H| \gg \Omega_B$ one can separate transverse ($\mathbf{S} - \mathbf{S^0} \perp \mathbf{H}$) and longitudinal ($\mathbf{S} - \mathbf{S^0} \parallel \mathbf{H}$) oscillations of spin. For a harmonic solution $\mathbf{S} - \mathbf{S^0} = \mathbf{s}\ e^{i\omega t}$ one can write

$$\left[-c_\perp^2\nabla^2 - (c_\parallel^2 - c_\perp^2)\nabla_j \hat{l}_j \hat{l}_k \nabla_k + \frac{\Omega_B^2}{2}\sin^2\beta_n\right] s_+ = \\ = \omega(\omega - \omega_L)\ s_+, \\ \left[-C_\perp^2\nabla^2 - (C_\parallel^2 - C_\perp^2)\nabla_j \hat{l}_j \hat{l}_k \nabla_k + \Omega_B^2\cos^2\beta_n\right] s_z = \\ = \omega^2\ s_z, \tag{6}$$

[1)]e-mail: vladislav.zavyalov@aalto.fi

where $s_+ = \frac{1}{\sqrt{2}}(s_x + is_y)$, β_n is an angle between $\hat{\mathbf{n}}$ and $\mathbf{H}$, the orbital anisotropy axis $\hat{l}_j = R_{aj}\hat{S}^0_a$, and

$$c_\perp^2 = \frac{\gamma^2\Delta^2}{\chi_B}(K - K'/2), \quad c_\parallel^2 = \frac{\gamma^2\Delta^2}{\chi_B}K,$$
$$C_\perp^2 = \frac{\gamma^2\Delta^2}{\chi_B}K, \quad C_\parallel^2 = \frac{\gamma^2\Delta^2}{\chi_B}(K - K'). \tag{7}$$

In the case of short wavelengths (when the spin changes on a much shorter distance than the texture) one can write spectra for plane waves with a wave vector $\mathbf{k}$:

$$c_\perp^2\ k^2 + (c_\parallel^2 - c_\perp^2)(\mathbf{k}\cdot\hat{\mathbf{l}})^2 + \frac{1}{2}\Omega_B^2\sin^2\beta_n = \omega(\omega - \omega_L),$$
$$C_\perp^2 k^2 + (C_\parallel^2 - C_\perp^2)(\mathbf{k}\cdot\hat{\mathbf{l}})^2 + \Omega_B^2\cos^2\beta_n = \omega^2. \tag{8}$$

Here the meaning of all parameters becomes clear: $c_\perp$ and $c_\parallel$ are velocities of transverse waves, propagating perpendicular and parallel to the $\hat{\mathbf{l}}$ direction; $C_\perp$ and $C_\parallel$ are the velocities of longitudinal waves; Ω_B is a frequency of the uniform longitudinal NMR in a texture with $\mathbf{n}||\mathbf{H}$.

The first equation in (8) describes transverse spin waves, which are similar to that in ferromagnets. In the presence of magnetic field it has two solutions $\omega(k)$, which are called acoustic (low ω) and optical (high ω) magnons. The second equation for longitudinal waves is unique for ^{3}He. Spin-wave spectrum in a uniform texture is presented on Fig. 1.

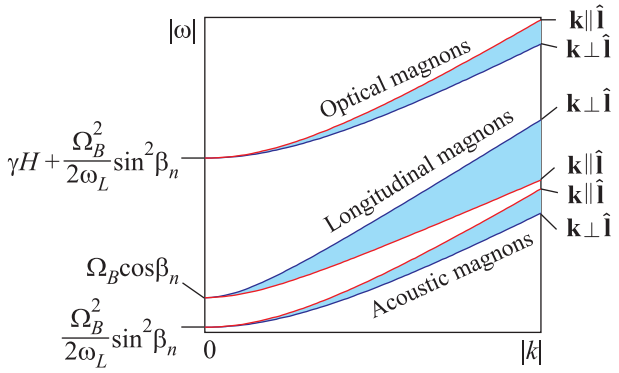

Fig. 1. Quasiclassical spin-wave spectrum in a uniform texture (β_n = const). There are two branches of transverse waves and one of longitudinal waves (8). Slopes of the branches at $k \to \infty$ are spin-wave velocities, they depend on the direction of propagation. Values at $k = 0$ give resonance frequencies in the uniform NMR

Gradient energy coefficients were calculated in Refs. [10, 11]. In particular, they depend on two antisymmetric Fermi-liquid parameters F_1^a and F_3^a. Neglecting the high-order parameter F_3^a, one has:

$$K_1 = K_2 = \frac{2}{\Delta^2}\ \frac{\hbar^2\rho}{40\ mm^*}\ \frac{(1+\frac{1}{3}F_1^a)(1-Y_0)}{1+\frac{1}{3}F_1^a - \frac{1}{5}F_1^a(1-Y_0)}, \tag{9}$$
$$K_3 = K_1\ \frac{1+\frac{1}{3}F_1^a}{1+\frac{1}{3}F_1^aY_0}.$$

Here m is the bare mass of ^{3}He, m^* is the effective mass of Fermi-liquid quasiparticles, ρ is the density of ^{3}He, and Y_0 is the temperature-dependent Yosida function.

Without Fermi-liquid corrections $K_1 = K_2 = K_3$ and one has

$$c_\perp/c_\parallel = \sqrt{3/4}, \quad C_\perp/C_\parallel = \sqrt{2}. \tag{10}$$

Schrödinger equation for optical magnons. In the case of optical magnons with $\omega \approx \omega_L$, in the texture where $\hat{\mathbf{n}}$ is almost parallel to $\mathbf{H}$, the first equation in (6) can be rewritten in a form of a Schrödinger equation for a magnon quasiparticle with an anisotropic mass:

$$\left[-\frac{\nabla_x^2 + \nabla_y^2}{2m_\perp} - \frac{\nabla_z^2}{2m_\parallel} + U\right] s_+ = E\ s_+. \tag{11}$$

Here complex value s_+ plays role of the magnon wave function, the energy is defined by the precession frequency $E = \hbar\omega$, and the values of the magnon mass are

$$m_\perp = \frac{\hbar\omega_L}{2c_\perp^2}, \quad m_\parallel = \frac{\hbar\omega_L}{2c_\parallel^2}. \tag{12}$$

Potential for magnons U is formed by the order parameter texture β_n and the magnetic field ω_L:

$$U = \frac{\hbar\Omega_B^2}{2\omega_L}\sin^2\beta_n + \hbar\omega_L. \tag{13}$$

In our setup we are able to create a harmonic trap for magnons in ^{3}He bulk far from cell walls. Using spectroscopy of levels in the trap we measure the magnon mass.

Experimental setup. We work with a ^{3}He sample confined in a long quartz tube (diameter 5.85 mm, length 15 cm) and cooled in a nuclear demagnetization cryostat. Temperature is measured by two vibrating tuning forks, located in the lower part of the experimental cell. Experiments are performed in the low temperature limit ($T = (0.13{-}0.20)\,T_c$), where such parameters as the gap Δ, Leggett frequency Ω_B, spin wave velocities $c_{\parallel,\perp}$, susceptibility χ_B do not depend on temperature. Pressures 0–29 bar are used.

The experimental volume is located near the upper end of the tube (Fig. 2). The NMR spectrometer includes a transverse pick-up coil made from copper. The coil is a part of the tuned tank circuit. Capacitor of the circuit is installed at the mixing chamber temperature.

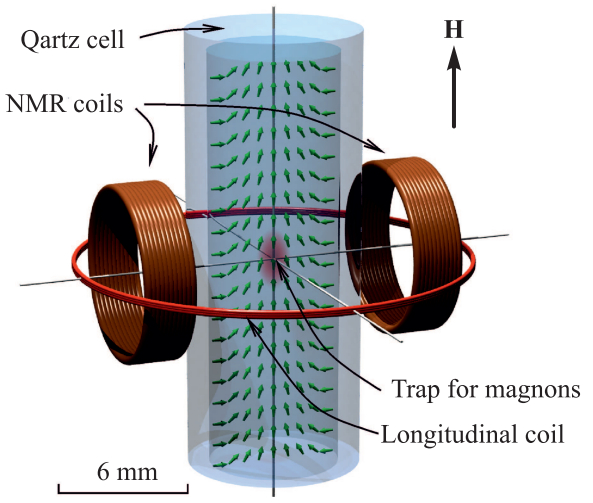

Fig. 2. Top part of the experimental cell. Arrows in the cell volume represent the order parameter texture ($\hat{\mathbf{l}}$ vector)

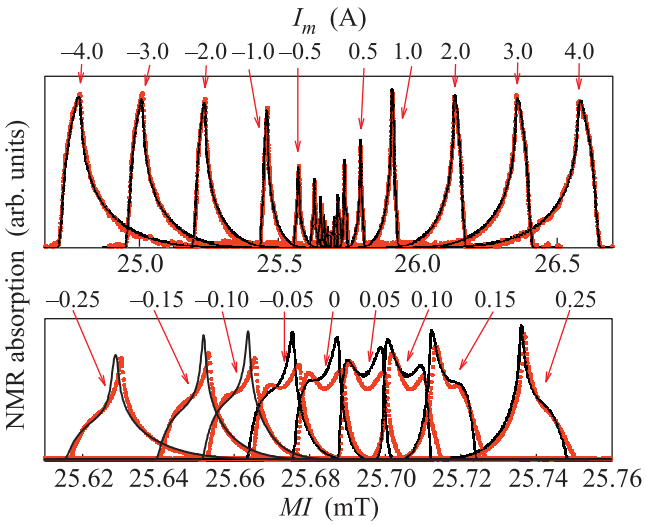

Fig. 3. Measured (points) and calculated (lines) NMR signals in normal ^{3}He at different values of I_m for the top spectrometer. Upper plot shows I_m in the range from -4 to 4 A, amplitude is multiplied by $|I_m|$; lower plot shows I_m in the range -0.25 A to 0.25 A

It can be switched to 8 different values changing the resonance frequency in the range 550–830 kHz, which corresponds to the NMR in ^{3}He at the magnetic field 17.0–25.5 mT. The Q value of the tank circuit is in the range 125–135 depending on the frequency.

In addition to the NMR solenoid, which produces a static magnetic field, a small superconducting longitudinal coil is used to create a minimum of the field at the center of the coil system. For the interpretation of the measurements it is important to know the field profile. We determine the profile using continues-wave (CW) NMR spectra measured in the normal ^{3}He (Fig. 3).

Magnetic field profile. In the simplest model the field of the main solenoid is uniform and proportional to the current I in it. The field of the longitudinal coil can be calculated as that of a current loop with the radius R_m, number of turns N_m, and current I_m.

Since both coils are superconducting, they distort the field. We have studied this effect numerically. Distortion of the main solenoid field can be accounted for by introduction of some additional current in the longitudinal coil $I_m^0 \propto I$. Distortion of the longitudinal coil field can be taken into account by introducing an additional uniform field proportional to I_m and adjusting the effective radius R_m of the loop.

We also introduce a tiny transverse gradient $g = \partial H/\partial x$ to explain the appearance of the double peak at $|I_m| < 0.1$ A. This effect is small and not important for most of our measurements (since it does not affect the quadratic terms in H), we use it only to improve fitting of the normal phase spectra.

The combined field is

$$H_z = M\, I - [M_0 + F(r,z) - F(0,0)]\; I_m^* + g\; x, \quad (14)$$

where $F(r,z)$ is the field of a circular loop with N_m turns, radius R_m and 1 A current and parameters have been found by fitting the normal ^{3}He CW NMR spectra:

$$M = 9.66914\ \text{mT/A},\ \ M^0 = 0.22305 \pm 0.00005\ \text{mT/A},$$
$$I_m^* = I_m + I_m^0,\ \ I_m^0 = -0.0292\ I,$$
$$R_m = 1.032 \pm 0.005\ \text{cm},\ \ g = 0.02\ \text{mT/cm}. \quad (15)$$

Minus sign in front of the second term in (14) shows that the longitudinal coil is directed opposite to the NMR solenoid to provide field minimum along the z-axis for a positive current I_m. Measured and calculated spectra in normal ^{3}He are shown in Fig. 3.

In experiments with trapped magnons only quadratic terms in the field distribution near the center of the experimental volume are important. Expansion of the analytical formula for the field of a current loop gives

$$F(r,z) = N_m\, \frac{\mu_0}{2R_m} \left(1 - \frac{3z^2}{2R_m^2} + \frac{3r^2}{4R_m^2}\right), \quad (16)$$

where μ_0 is vacuum permeability. Note that the ratio of quadratic terms of H_z in the z and r direction equals -2. This comes from the Maxwell equations and should be valid for any field distribution with this kind of symmetry. Our model for the field profile near the center gives

$$H_z = H_0 - M_r(r^2 - 2z^2)I_m^*, \quad (17)$$

where $M_r = 3N\mu_0/8R_m^3 = 0.1652 \pm 0.0024$ mT/A/cm^2 and H_0 is the field in the center.

Magnon spectra measurement. In our cylindrical cell order parameter of ^{3}He–B forms a so-called "flare-out" texture [12]. Near the cell axis the angle β_n can be approximated by a linear function of radial coordinate, $\beta_n(r) \approx \beta_n' r$. Together with the quadratic field profile (17) this results in a harmonic trap for magnons. The potential (13) can be written in the form

$$U = \hbar\omega_0 + m_\parallel \frac{\omega_z^2 z^2}{2} + m_\perp \frac{\omega_r^2 r^2}{2}, \qquad (18)$$

where

$$\omega_0 = |\gamma| H_0, \quad \omega_z^2 = 8c_\parallel^2 \frac{M_r I_m^*}{H_0},$$
$$\omega_r^2 = 2\left(\frac{c_\perp \Omega_B \beta_n'}{\gamma H_0}\right)^2 - 4c_\perp^2 \frac{M_r I_m^*}{H_0}. \qquad (19)$$

We can observe only axially symmetric and z-even eigenstates in the harmonic potential, since they have non-zero total transverse magnetization. Corresponding frequencies are

$$2\pi f_{(n_r,n_z)} = \omega_0 + (2n_r + 1)\,\omega_r + (n_z + 1/2)\,\omega_z, \quad (20)$$

with $n_r = 0, 1, 2, \ldots$ and $n_z = 0, 2, 4, \ldots$

We use pulsed NMR to populate a few lowest levels in this harmonic trap (Fig. 4). If the number of magnons

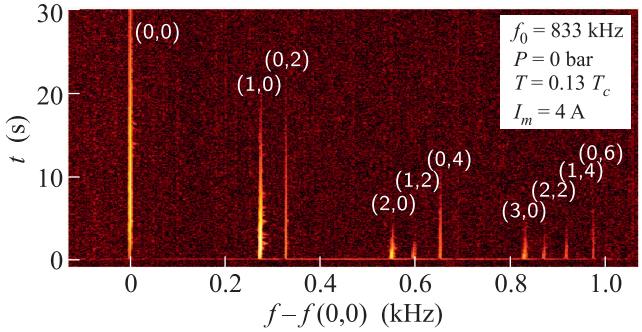

Fig. 4. Excitation of magnon levels in pulsed NMR. Color-coded amplitude of the Fourier transform of the signal from the pick-up coil is plotted as a function of time. A pulse of 0.96 ms duration excites a wide range of levels, seen as vertical lines. Levels are marked by quantum numbers (n_r, n_z)

in the system is small enough, interaction between the levels is negligible and multiple states can be resolved in the measurement using Fourier transform as in Fig. 4. We measure differences $f_{(n_r,n_z)} - f_{(0,0)}$ between higher levels and the ground level. This can be done with a precision better than 1 Hz. The measurements are repeated as a function of the longitudinal coil current I_m. With this procedure we separate the magnetic part of the potential which depends on I_m from the textural part. In Fig. 5 an example of such measurement is presented. Data are fitted using the resonant condition (20) with frequencies (19). We use only $n_r = 1$ and $n_z = 2$ states at $I_m > 0.5$ A to reduce anharmonic effects which grow with increasing spatial extent of the standing spin wave.

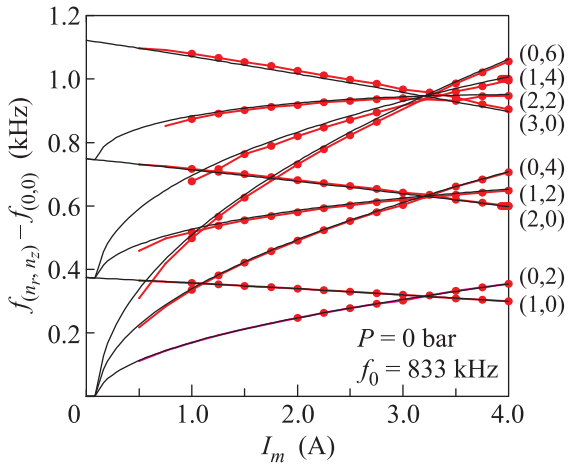

Fig. 5. An examples of spectra measurements. Differences between excited levels and the ground level, $f_{(n_r,n_z)} - f_{(0,0)}$ are plotted as a function of I_m. Whole set of lines is a single fit to Eq. (20). Only (1,0) and (0,2) states are used to find the fit parameters

We have found that the spectrum can be affected by textural defects, created when ^{3}He is cooled down from the normal phase [13]. Fig. 6 shows the magnon spectra measured in textures with and without defects. It is possible to remove defects by applying a large NMR pumping for a period of a few seconds.

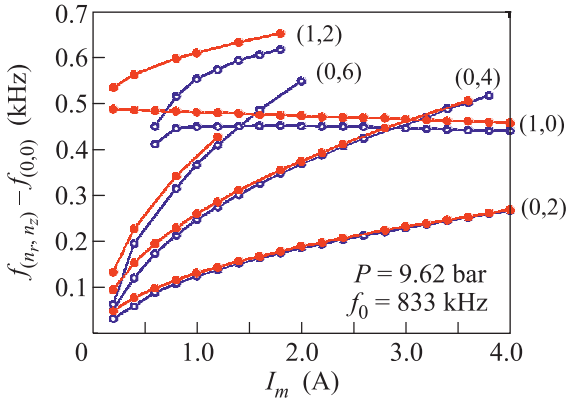

Fig. 6. Spectra measured in a texture with and without defects (open and filled circles correspondingly)

We have done spectra measurements for NMR frequencies $f_0 = (550{-}830)$ kHz and pressures $P = (0{-}29)$ bar. We fit the data using four parameters: $M_r c_\parallel^2$, $M_r c_\perp^2$, $c_\perp \Omega_B \beta'_n$, and I_m^0. The first two parameters describe the magnetic part of the potential, they are responsible for the axial and radial level dependence on I_m. Using these parameters and the M_r constant (17) one can find spin wave velocities. As expected, they do not depend on the frequency of the measurements. The pressure dependence is shown on Fig. 7. Accuracy of $c_\parallel$ measurement is much better then that of $c_\perp$ because axial levels have stronger dependence on I_m. The bad texture also has a smaller effect on it. Theoretical values, calculated using (7) and (9) are shown by dashed lines, the ratio $c_\parallel/c_\perp$ is presented on the inset of the figure. The smoothed measured values can be represented as (solid lines in the figure):

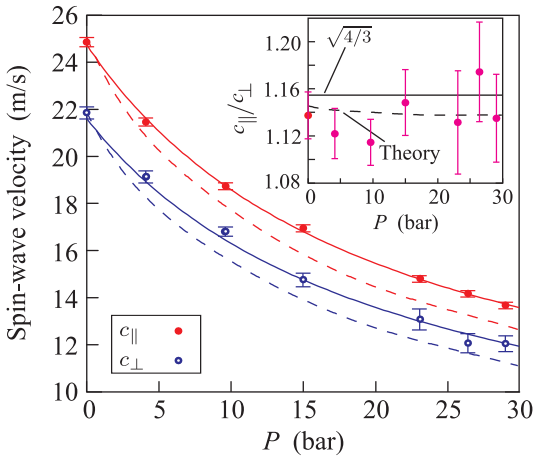

Fig. 7. Spin-wave velocities as a function of pressure. Filled and open circles with error bars show measured values of $c_\parallel$ and $c_\perp$. Dashed lines are theoretical values (7), solid lines are approximations (21). In the inset – the ratio $c_\parallel/c_\perp$ is plotted

$$c_\parallel(P\,[\text{bar}]) = \frac{387}{20.544 + P} + 5.94\ [\text{m/s}], \qquad (21)$$

$$c_\perp(P\,[\text{bar}]) = \frac{348}{21.138 + P} + 5.13\ [\text{m/s}]. \qquad (22)$$

The third fitting parameter, $c_\perp \Omega_B \beta'_n$ describes textural part of the radial potential, which does not depend on I_m. It gives us information about the texture close to the cell axis. The detailed structure of the texture obtained from the magnon spectra measurements will be published elsewhere. The last fitting parameter, I_m^0 is proportional to the NMR frequency and does not depend on pressure. Its value is given by (15).

Fermi-liquid parameter F_1^a. We can use expressions (7) and (9) to calculate spin-wave velocities in in the whole range of temperatures and pressures. Values of susceptibility χ_B and effective mass m^* are known reasonably well [14]. For theoretical curves in Fig. 7 we use value of F_1^a from [15]. It was found using normal ^{3}He specific heat measurements at relatively high temperatures (20–100 mK), where the Fermi-liquid approximation might not be very accurate. Higher-order Fermi-liquid parameters were neglected in that work. Other measurements of F_1^a [16, 17] claim even less accuracy. We have found F_1^a from our measured values of the spin-wave velocities (see Fig. 8). In the calculation we used Eq. (9) which was obtained in the weak-coupling approximation and neglects high-order Fermi-liquid parameters. Our results can be approximated as

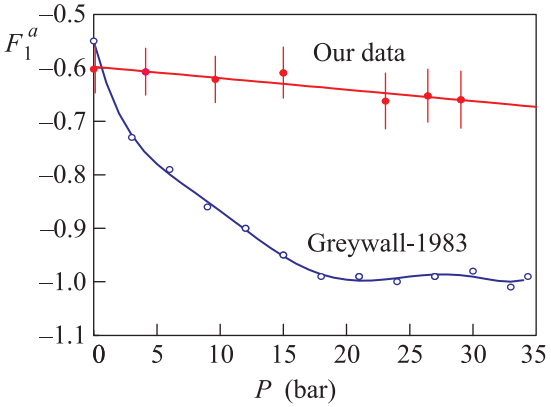

Fig. 8. Fermi-liquid parameter F_1^a as a function of pressure. Values restored from our spin-wave velocity measurements (Fig. 7) are shown by filled circles. The error bars show statistical uncertainty from the measurements, possible systematic error from ignoring high-order Fermi-liquid parameters and strong-coupling effects is not included. Open circles are measurements from [15]

$$F_1^a(P\,[\text{bar}]) = -0.598 - 0.00214\ P. \qquad (23)$$

This pressure dependence is much weaker than that found in Ref. [15]. The discrepancy at high pressures might originate in the strong-coupling effects which are not included in the used theoretical model.

Conclusion. In this paper we have presented our measurements of spectra of magnons in a magneto-textural trap in ^{3}He–B. The trap size can be controlled by the magnetic field, which allowed us to separate the magnetic and textural effects on the magnon levels in the trap and to measure spin-wave velocities. Values of the spin-wave velocities determine anisotropic magnon mass tensor and can be used to find Fermi-liquid parameter F_1^a. These new data could be used in future to refine values of other ^{3}He–B parameters, including properties of the orbital order-parameter texture and the

magnetic relaxation properties like spin diffusion. The latter is essential for application of trapped magnons as a self-calibrating thermometer in a microkelvin regime.

We thank G.E. Volovik for useful discussions. This work has been supported in part by the Academy of Finland (project # 250280), and by the facilities of the Cryohall infrastructure of Aalto University. P.J.H. acknowledges financial support from the Väisälä Foundation of the Finnish Academy of Science and Letters. S.A. acknowledges financial support from the Finnish Cultural Foundation.

1. T. Mizushima, Y. Tsutsumi, M. Sato, and K. Machida, J. Phys. Cond. Matter **27**, 113203 (2015).
2. Yu. M. Bunkov and G. E. Volovik, *Spin superfluidity and magnon Bose-Einstein condensation*, in: *Novel Superfluids*, ed. by K. H. Bennemann and J. B. Ketterson, International Series of Monographs on Physics 156 (2013), v. 1, ch. 4, p. 253.
3. E. V. Surovtsev and I. A. Fomin, JETP Lett. **90**, 211 (2009).
4. V. V. Zavjalov, S. Autti, V. B. Eltsov, P. J. Heikkinen, and G. E. Volovik, arXiv:1411.3983 (2014).
5. S. Autti, Yu. M. Bunkov, V. B. Eltsov, P. J. Heikkinen, J. J. Hosio, P. Hunger, M. Krusius, and G. E. Volovik, Phys. Rev. Lett. **108**, 145303 (2012).
6. V. B. Eltsov, R. de Graaf, M. Krusius, and D. Zmeev, J. Low Temp. Phys. **162**, 212-225 (2011).
7. V. B. Eltsov, P. J. Heikkinen, and V. V. Zavjalov, arXiv:1302.0764 (2013).
8. P. J. Heikkinen, S. Autti, V. B. Eltsov, R. P. Haley, and V. V. Zavjalov, J. Low Temp. Phys. **175**, 681-705 (2014).
9. S. Theodorakis and A. L. Fetter, J. Low Temp. Phys. **52**, 559 (1983).
10. M. C. Cross, J. Low Temp. Phys. **21**, 525 (1975).
11. M. Dörfle, Phys. Rev. B **23**, 3267 (1981).
12. H. Smith, W. F. Brinkman, and S. Engelsberg, Phys. Rev. B **15**, 199 (1977).
13. P. J. Hakonen, M. Krusius, M. M. Salomaa, R. H. Salmelin, J. T. Simola, A. D. Gongadze, G. E. Vachnadze, and G. A. Kharadze, J. Low Temp. Phys. **76**, 225 (1989).
14. D. Vollhardt and P. Wölfle, *The Superfluid Phases of helium 3*, Taylor and Francis, London (1990).
15. D. S. Greywall, Phys. Rev. B **27**, 2747 (1983).
16. L. R. Corruccini, D. D. Osheroff, D. M. Lee, and R. C. Richardson, Phys. Rev. Lett. **27**, 650 (1971).
17. D. D. Osheroff, Physica B **90**, 20 (1977).